Supporting Information (SI)

New insights into highly efficient reduction of CO_2 to formic acid by using zinc under mild hydrothermal conditions: a joint experimental and theoretical study

Xu Zeng,[a] Makoto Hatakeyama,[b] Koji Ogata,[b] Jianke Liu,[c] Yuanqing Wang,[b] Qi Gao,[d] Katsushi Fujii,[e] Masamichi Fujihira,[d] Fangming Jin*[a] and Shinichiro Nakamura*[b]

[a] School of Environmental Science and Engineering, Shanghai Jiao Tong University, Shanghai, 200240, China.

[b] RIKEN Research Cluster for Innovation Nakamura Laboratory, Wako, Saitama, 351-0198, Japan.

[c] College of Environmental Science and Engineering, Tongji University, Shanghai, 200092, China.

[d] Science and Technology Research Center, Mistsubishi Chemical Group, Yokohama, 227-8502, Japan.

[e] Research Center for Advanced Science and Technology, University of Tokyo, Tokyo, 153-8904, Japan.

Corresponding Author:

E-mail: fmjin@sjtu.edu.cn (Fangming Jin); snakamura@riken.jp (Shinichiro Nakamura).

Fax/Tel: +86-21-54742283 (Fangming Jin); +81-048-467-9477 (Shinichiro Nakamura).

Experimental information

Most of the experiments were conducted using batch reactors that consisted of SUS 316 tubing (9.525 mm o.d., 1-mm wall thickness and 120-mm length) with two end fittings, giving an inner volume of 5.7 ml. Details of apparatus have been described[1-3]. The typical reaction procedure used was as follows: a desired amount of $NaHCO_3$ and Zinc powders and 2 ml deionized water were loaded into the reactor

that occupied about 35% of the total reaction volume. When CO_2 gas was used for the reaction, a valve was connect to the reaction tube to control the injected gas amount, as shown in Figure SI-1. Also the gas pressure was controlled, so that the molar amount can be calculated. Pressures at the highest temperature of 573 K would be around 8.6 MPa according to the loading limit conditions. After loading, the reactor was sealed and then immersed into a salt bath, which had been preheated to the desired temperature. The typical heat-up time required to raise the temperature of the reactor from 20 to 573 K was about 20 s. After the preset reaction time, the reactor was removed from the salt bath and immediately immersed in a cold-water bath. The reaction time was defined as the time period during which the reactor was kept in the salt bath.

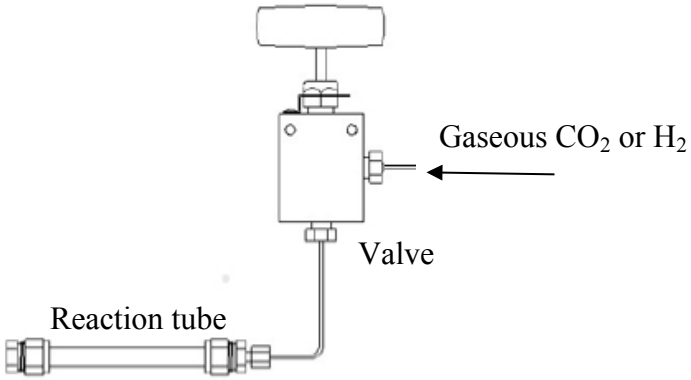

Figure S1. Reaction equipment for the reaction with gas.

After the reactors were cooled, the liquid and solid samples were collected and treated by washing or diluting with water or ethanol when required for analysis. Liquid samples were analyzed by HPLC, GC/FID/MS, and XRD, respectively. HPLC analysis was performed on KC-811 columns (SHODEX) with a HPLC system (Agilent Technologies 1200), which was equipped with a tunable UV/Vis absorbance detector adjusted at 210 nm. Mobile phase was 2 mmol/L $HClO_4$ solution at an isocratic flow rate of 1.0 ml/min. Quantitative estimation of formic acid concentration was based on the average value obtained from at least three samples by HPLC analysis. For GC/MS analysis, a Hewlett-Packard model 7890A Gas Chromatograph system equipped with a model 5975C Mass Selective Detector was used. The initial temperature of oven in the gas chromatograph was kept at 313 K for 1 min and then

programmed to increase at a rate of 7 °C/min to a final temperature of 503 K that was held at this value for 20 min. Samples were separated with a HP-INNOWAX polar capillary column (25 m long, 0.25 mm i.d., 0.5 μm film thickness) using helium as carrier gas. For GC/FID analyses, a Hewlett-Packard model 7890 Series II Gas Chromatograph was used with analytical conditions being the same as those used for the GC/MS method. Gas samples were analyzed with a GC system (HP-5890 Series II), equipped with a HP-1 packing column (30 m×0.25 mm i.d.) and a TCD detector. Solid samples were washed with deionized water several times and dried in air and then characterized by X-ray diffraction (XRD) (D/MAX2550, Rigaku, and Bruker D8 Advance) using Nifiltered Cu *Kα* radiation at an acceleration voltage of 40 KV and emission current of 100 mA for D/MAX2550 and 40 mA for Bruker D8 Advance, respectively. The step scan covered angles of 5-70 ° (2θ), at a rate of 10 °/min for D/MAX2550, Rigaku and 1.2°/s for Bruker D8 Advance, respectively.

References

1. F. Jin, J. Cao, H. Enomoto, T. Moriya, *J. Supercritical Fluids* **2001**, 19, 251.
2. F. Jin, T. Moriya, H. Enomoto, *Environ. Sci. Technol.* **2003**, 37, 3220.
3. F. Jin, Z. Zhou, T. Moriya, H. Kishida, H. Higashijima, H. Enomoto, *Environ. Sci. Technol.* **2005**, 39, 1893.

Analysis results of liquid and solid samples after the reaction

XRD pattern of solid products is shown in Figure S2. All Zn was converted into ZnO after hydrothermal reaction. Actually, Zn can react with H_2O drastically at high temperature. Even within 5 min, above 95% of the total Zn can be oxidized to ZnO at 573 K.

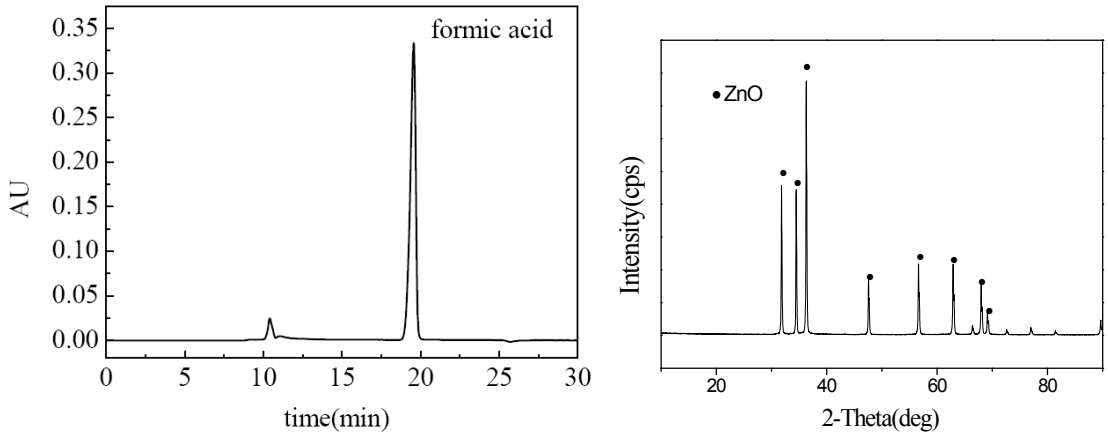

Figure S2. HPLC Chromatography of liquid sample and XRD pattern of solid sample after reaction (at 573 K for 120 min, $NaHCO_3$ 1 mmol; Zn 6 mmol; H_2O 111 mmol).

Experiments with ZnO 6 mmol and in the presence or absence of H_2 6 mmol were performed, to compare the formic acid with the experimental results from same molar amounts of Zn. With ZnO 6 mmol and H_2 6 mmol, only 13% yield of formic acid was obtained. When CO_2 is absorbed into NaOH solution, the yield of formic acid increased. The results show that the yields of formic acid increase, if there is enough waiting time even at room temperature, similarly with the conditions of Zn.

Table S1. Yields of formic acid (Y_{HCOOH}) with ZnO 6mmol

Entry	$NaHCO_3$ /mmol	CO_2 /mmol	NaOH /mmol	H_2 / mmol	H_2O / mmol	Y_{HCOOH} / %
5	1	0	0	6	111	13
6	1	0	0	6	0	0
7	0	1	1	6	111	3
7.(1)	0	1	1	6	111	12
7.(2)	0	1	1	6	111	13

To investigate the effects of HCO_3^- and CO_3^{2-} and metal cation on the yield of formic acid, experiments with $KHCO_3$ and K_2CO_3 were performed. As shown in Figure 3, the yields of formic acid from $NaHCO_3$ and $KHCO_3$ were much higher than the yields from Na_2CO_3 or K_2CO_3. The results suggest that formic acid can be produced with high yield from HCO_3^-, not from CO_3^{2-}. From Figure 3, there was almost no obvious difference between the yields from $NaHCO_3$ and $KHCO_3$, either from Na_2CO_3 and K_2CO_3, which indicates that Na^+ and K^+ have almost no effect on the production of formic acid.

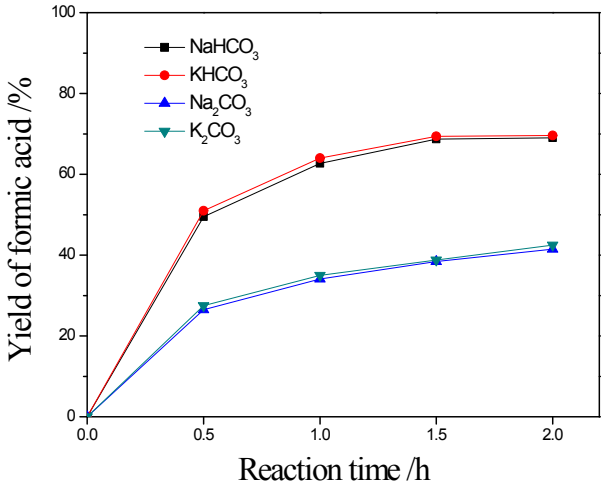

Figure S3 Yield of formic acid with different carbonates (Zn 6 mmol, Carbonate 1mmol, H2O 111 mmol, Temp. 573 K).

Details of the exhausted search calculations

As shown in Scheme S1, the most stable cluster of Zn_5 forms a trigonal bipyramid (TBP). We used the Zn5 TBP throughout our calculations. It provides vertex, linear, and surface environments. Around the Zn_5 cluster, various sites are possible; five sites at the Zn vertex positions (two apical and three equatorial), nine sites on the bonds connecting two Zn atoms, and six sites at the center of the triangles consisting of three Zn atoms. Of these 20 sites, taking symmetry of the Zn_5 into account, we considered that five categories of the sites could generate initial geometries for the quantum chemical optimization. The positions to put the fragments as an initial structure are shown in Scheme S1 as yellow balls. The vertex Zn atoms and their bonds are shown in black and gray, respectively. Positions 1 and 2 are the vertexes of the Zn_5 cluster, Positions 3 and 4 are the centers of two Zn atoms, and position 5 is the center of mass of the triangle of three Zn atoms (see Scheme S1).

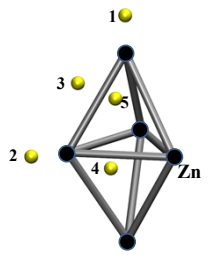

Scheme S1 Zn_5 cluster with 5 possible positions

Onto the five sites thus selected, the decomposed fragments from two waters are distributed as shown by the amount numbers listed in Table 3, where the amount numbers are for each mode. Two waters can be fragmented in various modes as shown by modes (1) ~ (6) in Table S2. The vertex sites (black in Scheme 3) are considered (i) bidentate or (ii) monodentate. The remaining three other sites (on a Zn…Zn line or a plane determined by three Zn atoms) are occupied only by O^{2-} ions or H_2O molecules because the trial calculations gave unstable bonding with H^+ or OH^- on these three sites.

(i) 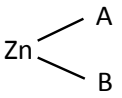

(A≠B): A and B are fragments selected from H^+, HO^-, or O^{2-}.

(ii) 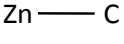

: C is a fragment selected from H^+, HO^-, O^{2-}, or H_2O.

Table S2 Fragments distribution modes on Zn5 cluster

Mode	Structures	Amounts
(1)	Zn_5, {H_2O, H_2O}	20
(2)	Zn_5, {H_2O, H^+, OH^-}	40
(3)	Zn_5, {H_2O, H^+, H^+, O^{2-}}	228
(4)	Zn_5, {H^+, OH^-, H^+, OH^-}	29
(5)	Zn_5, {H^+, OH^-, H^+, H^+, O^{2-}}	179
(6)	Zn_5, {H^+, H^+, O^{2-}, H^+, H^+, O^{2-}}	363
Total		859

Initial geometries of fragments and Zn cluster were constructed as following. For the fragments H^+, HO^- and O^{2-}, each is located on the site so that chemical bond is formed with 1.0 Å as its initial length (distance to Zn). For non-fragmented H_2O molecule, not chemical bond, but weak interaction (non-bonded) is considered. Oxygen atom of water has three types of interactions to Zn5 cluster ; (1) with a distance of oxygen and Z vertexes (yellow 1 or 2), (2) with a distance between oxygen and the center of Zn-Zn (yellow 3 or 4), and (3) with a distance of the center of mass of the triangle (yellow 5). The

distances are changed from 1.0 Å to 3.0 Å with the interval of 0.1 Å. In each, we optimized the position of hydrogen atoms. The geometries of preliminary structures thus generated are optimized. Structures with the lowest energy were obtained.

We used these optimized structures as the initial structures of the intermediate searches. The structures on the 15 remaining sites other than above 5 sites were generated by rotating the initial structures. All the possible structures generated from two H_2O molecules (see mode (1) ~ (6) in Table 3) were generated from the representative fragment structure in consideration of the symmetry of the Zn_5 cluster. A total of 859 structures were generated, eventually all the structures were optimized without any geometry constrains.

Pattern of $NaHCO_3$ and $2{\cdot}H_2O$ decompositions

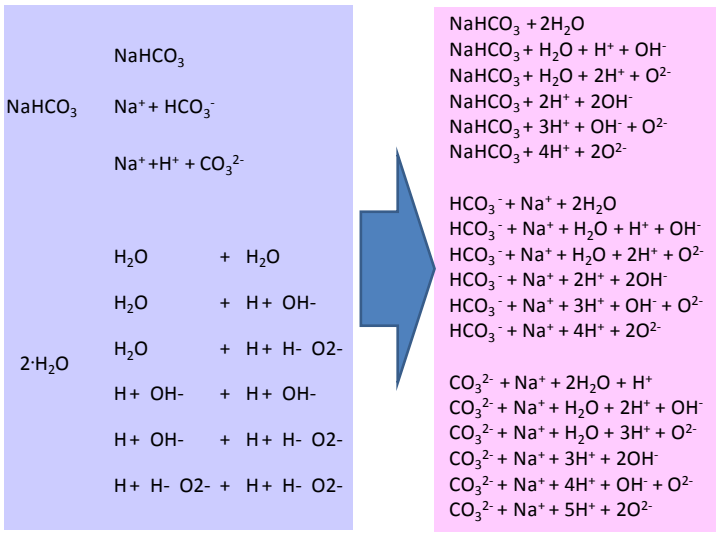

Generation of the all possible structures

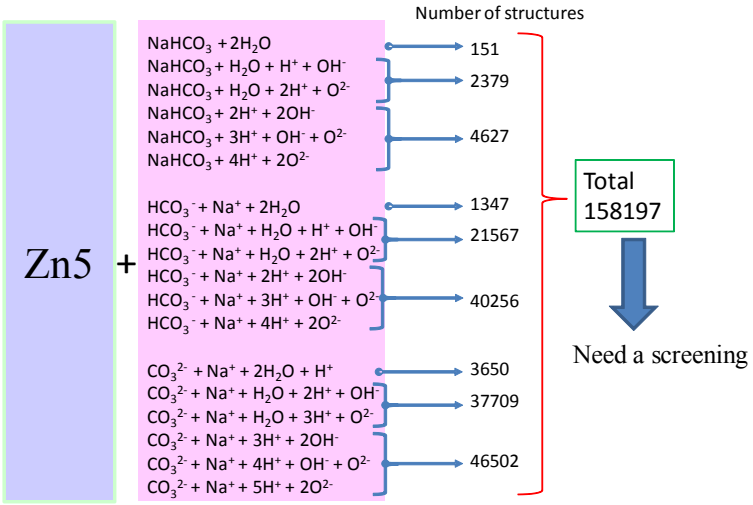

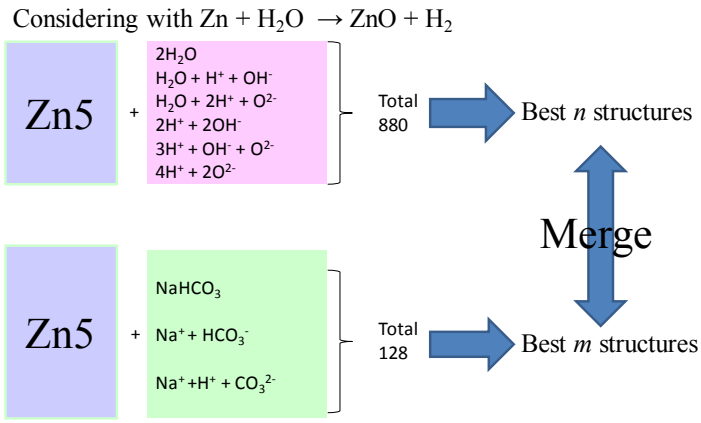

Figure S4. Screening method for the calculation test.

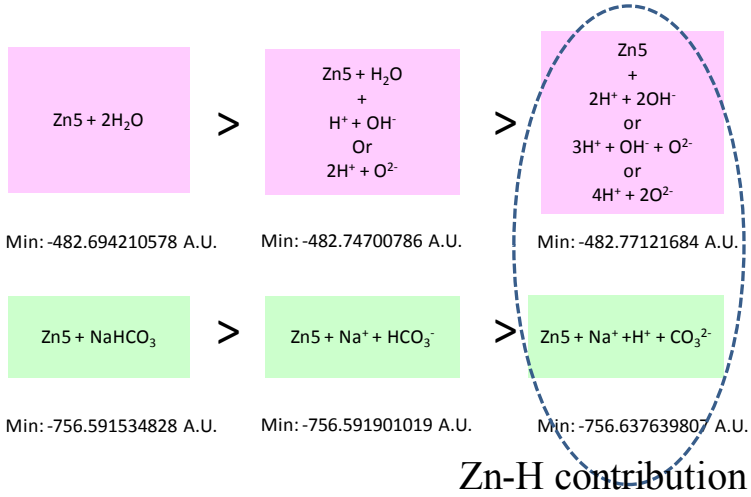

Figure S5. Results of screening test.

Calculated energies for Zn_5 and two H_2O

Figure S4 shows the relative thermodynamic stability of the system consisting of Zn_5 clusters and the fragments of two H_2O molecules. The most stable structures in each mode (of Table S2) are shown in Figure S4. The energies in kcal/mol are relative to the system of two H_2O molecules (non-fragmented mode (1) of Table S2) on the Zn_5 cluster. All the geometrical parameters were fully optimized, and the harmonic vibrational frequencies were obtained analytically to be minimum at the optimized structures.

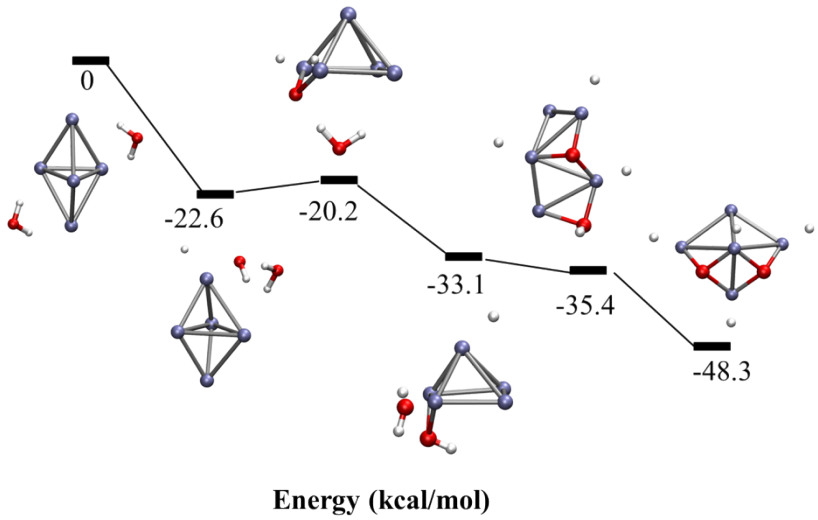

Figure S6. Energy of each mode relative to the energy of the system with a Zn_5 cluster and non-fragmented two H_2O system.

Results show that the energy of the Zn_5 cluster with fragmented H_2O is stable. For instance, the energy of {H_2O, OH^-, H^+} (−22.6 kcal/mol) is lower than that of {H_2O, H_2O} (0 kcal/mol). Increasing the number of H^+, more stable structures are obtained. For instance, the energy of {O^{2-}, H^+, H^+, O^{2-}, H^+, H^+} (−48.3 kcal/mol) is lower than that of {H_2O, OH^-, H^+} (−20.2 kcal/mol). Furthermore, in the case that two O^{2-} ions are generated, the most stable case is obtained. From these results of Zn5 + $2H_2O$ reactions, we can expect that $2H_2O$ molecules will be decomposed and form Zn–H and Zn-O-Zn units. Therefore, from the viewpoint of relative thermodynamic stability, it is suggested that Zn–H can exist in the formic acid formations if the activation energy is not too high. In the next section, we will examine this transition state (TS) by using a Zn_5 cluster and one H_2O molecule.

We used Zn_5, $NaHCO_3$, two H_2O molecules to conduct the quantum chemistry calculation. First, we considered different decomposition patterns of $NaHCO_3$ and two H_2O molecules, as shown in Figure S4. $NaHCO_3$ has three patterns and two H_2O molecules have six patterns, therefore, we can obtain 18 patterns with decomposed $NaHCO_3$ and two H_2O molecules. Secondly, as discussed in the article, the decomposed species was mounted to the different sites on Zn_5 surface. The total number of all possible patterns with Zn_5, $NaHCO_3$ and two H_2O molecules is 158197. Indeed, we must perform a screening.

For further calculations, we discussed with Zn_5 and two H_2O molecules, Zn_5 and $NaHCO_3$ separately. Then we can obtain 880 and 128 patterns for each. Based on this screening method, quantum chemical calculations are performed. The results of free energy are shown in Figure S5. These results suggest that Zn–H species is more stable and possible as a intermediate for the formic acid formation.

Calculated free energy for the production of Zn–H

The relative free energy and transition state for the formation of Zn–H at 573 K were calculated by using the model Zn_5 cluster and H_2O. Transition states were located by full optimizations and characterized by a single imaginary frequency. The initial guess of the transition states was obtained by a quadratic synchronous transit approach to access at the quadratic region of the transition state. Considering the structure of Zn_5 model, four patterns of H_2O position—patterns 1 and 2 for a bidentate mode on Zn (H–Zn–OH), and patterns 3 and 4 for monodentate modes of H and OH on the different Zn vertexes—were considered (Figure S5). The results suggest that the Zn–H species can be produced from Zn and water molecule, once enough energy to pass the TS is provided, since the activation energies for each pattern are not too high and are accessible under the current experimental conditions.

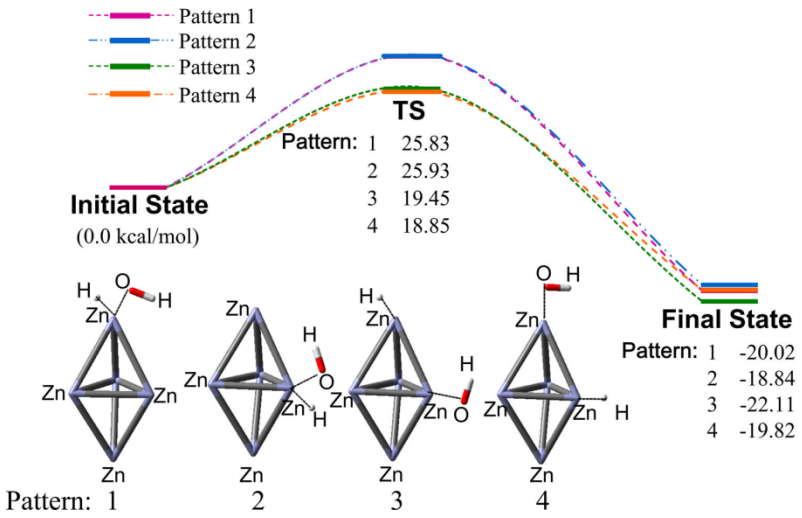

Figure S7. Calculated free energy at 573 K for the Zn–H formation in four patterns.

Cartesian coordinates of Zn5 and TS (pattern I)

Zn_5 cluster

Atomic	Coordinates (Angstroms, X, Y, Z)		
Zn	1.056665	4.429358	3.057187
Zn	2.790376	6.266011	3.639070
Zn	3.593922	4.362572	2.339505
Zn	3.126160	4.085140	4.713062
Zn	5.248952	5.353276	4.000676

The transition state

Atomic	Coordinates (Angstroms, X, Y, Z)		
Zn	-0.392421	5.446900	2.864269
Zn	1.095263	6.619196	4.850875
Zn	1.171176	3.375844	2.100529
Zn	1.249483	3.926513	4.764273
Zn	2.582008	5.636761	2.764834
H	1.753174	3.285656	0.242923
C	1.569839	1.794765	0.144660
O	0.952472	1.528999	1.327305
O	2.978819	1.412545	0.269271
O	1.043259	1.556549	-0.983110
H	3.261678	1.366544	-0.668685

Geometries of TS for four patterns of the Zn–H species formation

Pattern 1

Zn	1.336997	3.486857	3.005453
Zn	2.291407	5.964228	3.843541
Zn	3.914838	4.132740	2.331540
Zn	3.271696	3.590001	5.098974
Zn	5.099101	5.691849	4.348591
H	-0.286839	2.951698	2.511473
O	-0.631998	4.302006	2.005434
H	-0.983786	4.609984	2.874927

Patter 2

Zn	1.416321	4.433877	2.726078
Zn	2.618932	6.572309	5.516918

Zn	4.211099	3.051994	2.558541
Zn	2.920818	3.776544	4.931651
Zn	3.897033	5.768927	3.105498
H	2.826175	2.486752	1.459627
O	1.377072	2.886855	1.238855
H	1.569512	3.441407	0.445521

Pattern 3

Zn	1.225135	4.355143	3.220386
Zn	3.413049	6.281727	3.227215
Zn	3.934581	3.649440	2.313923
Zn	3.588419	4.176874	5.086387
Zn	6.086949	5.116785	3.755972
H	0.472582	3.338111	5.218662
O	0.118156	2.883097	6.041484
H	0.451716	1.975875	5.920244

Pattern 4

Zn	1.174984	3.923047	3.059787
Zn	2.646358	6.017502	3.991574
Zn	3.634869	3.661813	2.158434
Zn	3.040193	3.411508	5.079101
Zn	5.134264	4.904899	4.036744
H	-0.555954	3.680589	2.897579
O	2.581452	2.510347	0.856016
H	2.218909	3.209853	0.267161

TS calculation of pattern II for formic acid formation (pattern II)

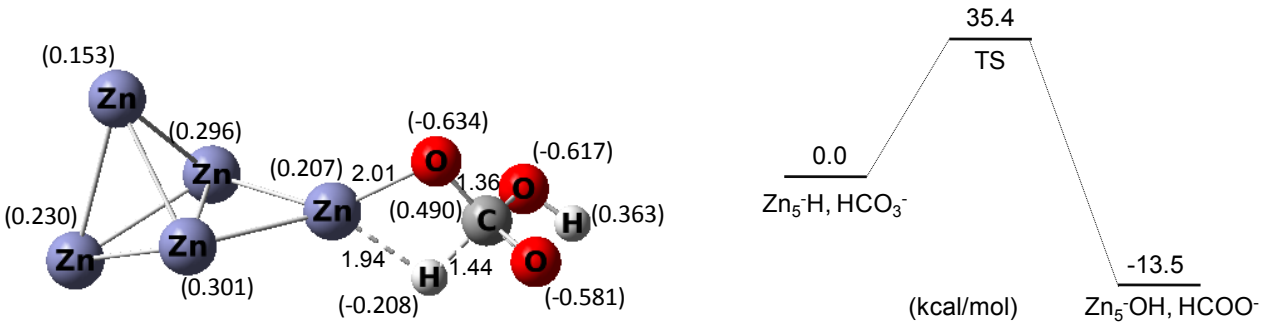

Figure S8. Activation energy of Zn-H + HCO_3^- → Zn_5-OH^- + $HCOO^-$ (pattern II).

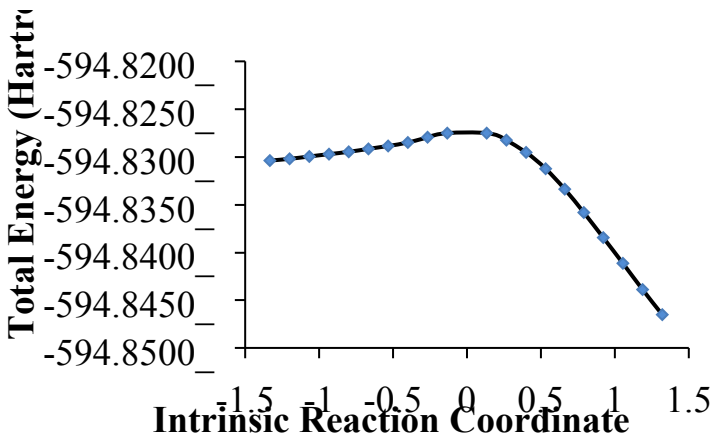

Figure S9. IRC calculation for TS (see Figure S8).

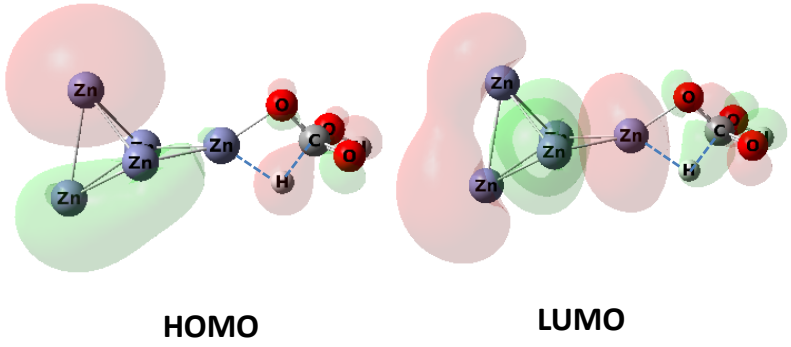

Figure S10. HOMO and LUMO orbital shapes of the TS shown in Figure S8.

Geometries of TS

Zn	-0.54571300	4.46433800	2.72516300
Zn	0.97620200	5.90328900	4.57752100
Zn	2.12056000	3.74989400	2.81623100
Zn	0.75411200	3.17423800	5.08941500
Zn	3.01103400	6.25099100	2.91132400
H	4.89686400	6.74356400	3.11996100
C	4.87069400	7.75593600	2.07906800
O	3.54368900	7.80268700	1.74266300
O	5.57883800	6.99256600	1.02774300
O	5.50598300	8.77429900	2.51683000
H	6.50699800	7.29659800	1.16034000

Calculation with large cluster of Zn20

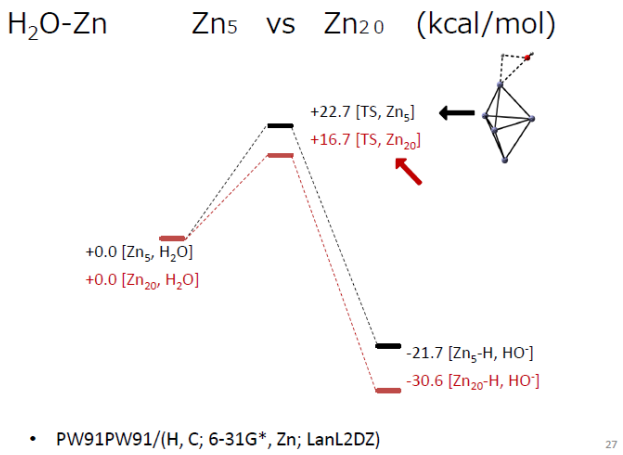

Figure S11. Comparison of Zn_5 and Zn_{20} cluster (Zn_{20} is shown in the figure below).

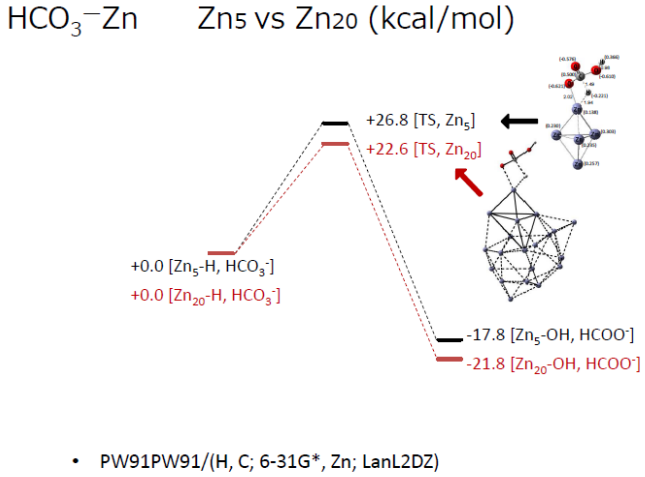

Figure S12. Comparison of Zn_5 and Zn_{20} cluster.

The structures of Zn_{20}-H_2O and H-Zn_{20}-HCO_3^- were obtained by three-stage processes; (i) optimization of Zn_{20}-cluster (ii) superposition of Zn_5-H_2O or H-Zn_5-HCO_3^- structures on the Zn_{20}-cluster (iii) constraint-optimization of Zn_{20}-H_2O and H-Zn_{20}-HCO_3^-. Stage (i) (Zn_{20}-optimization) was performed by DFT-PW91/LanL2DZ. The initial structure was chosen from the molecular dynamics of Zn_{20}-cluster by respecting the potential energy and early theoretical study on Zn_n (n=2-20) clusters [J. Wang, et al. *Phys. Rev. A*, 2003, **68**, 013201]. The dynamics was calculated by density functional tight binding (DFTB) [B. Aradi, et al., *J. Phys. Chem.*, A, 2007, **116**(26), 5678] method. Stage (ii)

(superposition of Zn_5-models on Zn_{20}-cluster) was performed by searching a hexahedron Zn_5 unit on the Zn_{20}-cluster. Among the Zn_5-unit, one Zn atom on the surface of Zn_{20}-cluster was used to adsorb H_2O, H or HCO_3^-. The adsorption distances and intra-molecular structures of those substrates were referred from the Zn_5-models. Stage (iii) (constraint-optimization) was performed by constraining the adsorption distances and intramolecular structures of substrates (H, H, HCO_3^-) and using DFT-PW91 functional.